Fundamentals of reservoir surface energy as related to surface properties, wettability, capillary action, and oil recovery from fractured reservoirs by spontaneous imbibition

DE-FC26-03NT15408

Quarterly Report
07/01/2004 – 9/30/2004

Norman R. Morrow, Principal Investigator
Herbert Fischer
Yu Li
Geoffrey Mason
Douglas Ruth
Siddhartha Seth
Peigui Yin
Shaochang Wo

October 2004

Submitted by:
Chemical & Petroleum Engineering
University of Wyoming
Dept. 3295, 1000 E. University Ave
Laramie, WY 82071

Disclaimer

This report was prepared as an account of work sponsored by an agency of the United States Government. Neither the United States Government nor any agency thereof, nor any of their employees, makes any warranty, express or implied, or assumes any legal liability or responsibility for the accuracy, completeness, or usefulness of any information, apparatus, product, or process disclosed, or represents that its use would not infringe privately owned rights. Reference herein to any specific commercial product, process, or service by trade name, trademark, manufacturer, or otherwise does not necessarily constitute or imply its endorsement, recommendation, or favoring by the United States Government or any agency thereof. The views and opinions of authors expressed herein do not necessarily state or reflect those of the United States Government or any agency thereof.

ABSTRACT

The objective of this project is to increase oil recovery from fractured reservoirs through improved fundamental understanding of the process of spontaneous imbibition by which oil is displaced from the rock matrix into the fractures. Spontaneous imbibition is fundamentally dependent on the reservoir surface free energy but this has never been investigated for rocks. In this project, the surface free energy of rocks will be determined by using liquids that can be solidified within the rock pore space at selected saturations. Thin sections of the rock then provide a two-dimensional view of the rock minerals and the occupant phases. Saturations and oil/rock, water/rock, and oil/water surface areas will be determined by advanced petrographic analysis and the surface free energy which drives spontaneous imbibition will be determined as a function of increase in wetting phase saturation. The inherent loss in surface free energy resulting from capillary instabilities at the microscopic (pore level) scale will be distinguished from the decrease in surface free energy that drives spontaneous imbibition.

A mathematical network/numerical model will be developed and tested against experimental results of recovery versus time over broad variation of key factors such as rock properties, fluid phase viscosities, sample size, shape and boundary conditions. Two fundamentally important, but not previously considered, parameters of spontaneous imbibition, the capillary pressure acting to oppose production of oil at the outflow face and the pressure in the nonwetting phase at the no-flow boundary versus time, will also be measured and modeled. Simulation and network models will also be tested against special case solutions provided by analytic models.

In the second stage of the project, application of the fundamental concepts developed in the first stage of the project will be demonstrated. The fundamental ideas, measurements, and analytic/numerical modeling will be applied to mixed-wet rocks. Imbibition measurements will include novel sensitive pressure measurements designed to elucidate the basic mechanisms that determine induction time and drive the very slow rate of spontaneous imbibition commonly observed for mixed-wet rocks. In further demonstration of concepts, three approaches to improved oil recovery from fractured reservoirs will be tested; use of surfactants to promote imbibition in oil wet rocks by wettability alteration: manipulation of injection brine composition: reduction of the capillary back pressure which opposes production of oil at the fracture face.

TABLE OF CONTENTS

INTRODUCTION 5
Objectives 5
TASKS 5
Progress BY TASK - Budget Period 1 7
Task 1. 7
Introduction 7
Experimental 7
Results and Discussion 9
Task 2. 11
Introduction 11
Experimental 11
Results and Discussion 14
Task 3. 17
Introduction 17
Experimental 20
Results and Discussion 22
Task 4 23
Introduction 23
Experimental 23
Results and Discussion 24
Task 5. 27
Introduction 27
Verification 27
Results and Discussion 37
Conclusions 37
REFERENCES 37

INTRODUCTION

Objectives

The long-range objective of this project is to improve oil recovery from fractured reservoirs through improved fundamental understanding of the process of spontaneous imbibition by which oil is displaced from the rock matrix into the fractures. Spontaneous imbibition is fundamentally dependent on the surface energy. An initial objective is to determine the surface energy and relate the dissipation of surface energy to the mechanism of spontaneous imbibition. A parallel objective is to model the mechanism of spontaneous imbibition by a combination of network analysis and numerical modeling. Also fundamentally important, but not previously considered, parameters of spontaneous imbibition, the capillary pressure acting to oppose production of oil at the outflow face and the pressure in the nonwetting phase at the no-flow boundary (in effect within oil in the non-invaded zone of the rock matrix) versus time, will also be measured and compared with values predicted by the mathematical model. The next objective is to measure surface energy and related spontaneous imbibition phenomena for mixed-wettability rocks prepared by adsorption from crude oil. The dissipation of surface free energy must then be related to oil production at mixed-wet conditions. The final objective is to apply the results of the project to improved oil recovery from fractured reservoirs in three ways: reduction of the capillary force that opposes oil production at the fracture face; change in wettability towards increased water wetness; identification of conditions where choice of invading brine composition can give improved recovery.

TASKS

Budget period 1, July 1, 2003 through June 30, 2005 – Ideas and Concept development: Fundamentals of Spontaneous Imbibition

Task 1. *Work of displacement and surface free energy.* Obtain complementary sets of capillary pressure drainage and imbibition data and data on changes in rock/brine, rock/oil, and oil/brine interfacial areas with change in saturation for drainage and imbibition for at least two rock types (sandstone and carbonate). Determine free-energy/work-of-displacement efficiency parameters for drainage and imbibition for at least two rock types so that changes in rock/wetting phase/nonwetting phase surface areas can be closely estimated from capillary pressure measurements.

Task 2. *Imbibition in simple laboratory and mathematical network models.* Study imbibition in at least three simple tube networks that can be modeled analytically to establish and/or confirm fundamental aspects of the pore scale mechanism of dynamic spontaneous imbibition with special emphasis on determining how spontaneous imbibition is initiated and the key factors in how the saturation profile develops with time. Incorporate rules developed from laboratory measurements on relatively simple networks into the design of a computational network model. Use the network model to obtain an account of the mechanism by which imbibition is initiated, the saturation profile is developed, and the rate of spontaneous imbibition in terms of the dissipation of surface free energy that accompanies change in saturation.

Task 3. *Novel observations on fluid pressures during imbibition and the mechanism of non-wetting phase production at the imbibition face.* Make novel observations on the imbibition mechanism including details of the mechanism of oil production at the outflow rock face and the change in the nonwetting phase pressure at the no-flow boundary of the core during the course of spontaneous imbibition for at least 16 distinct combinations of rock/ fluid properties.

Task 4. *Network/numerical model and new imbibition data.* Develop a numerical simulator specifically designed for spontaneous imbibition. Incorporate the network model to obtain a network/numerical model that includes matching the measured pressure in the nonwetting phase at the no-flow boundary, and the pressure that opposes production of oil at the open rock face. Imbibition data will be obtained for at least 10 rocks with over six-fold variation in permeability, and at least 6 orders of magnitude variation in viscosity ratio, and at least 10 variations in sample size, shape, and boundary conditions.

Task 5. *Comparison with similarity solutions.* Compare results given by simulation with special case analytic results given by similarity solutions for spontaneous imbibition for at least five distinct cases of rock and fluid properties.

Budget Period 2, July 1, 2005 through June 30, 2008 - Demonstration of concept: Application to mixed wettability rocks and improved oil recovery from fractures reservoirs.

Task 6. *Rock preparation and Work of displacement and surface areas*
Obtain a range of rock types and identify and obtain crude oils that induce stable mixed wettability. Prepare at least 25 rocks with mixed wettability through crude oil/brine/rock interactions.
Determine work of displacement for drainage and imbibition and measure the variation in rock/brine, rock oil, and oil/brine interfacial areas during the course of drainage and imbibition for at least two examples of mixed wettability.

Task 7. *Novel imbibition measurements on mixed-wet rock and network models.* Obtain, for at least six mixed-wet rocks, spontaneous imbibition data that includes measurements of the nonwetting phase pressure at the no-flow boundary, observations on the capillary pressure that resists production at the open rock face.

Task 8. *Application of network/numerical model to mixed wet rocks.* Use network models to relate dissipation of surface energy to rate of spontaneous imbibition and to account for the frequently observed induction time prior to the onset of spontaneous imbibition into mixed wettability rocks.

Task 9. *Increased oil recovery by spontaneous imbibition.* The mechanism of increased recovery from mixed wet rocks by use of surfactants that promote spontaneous imbibition by favorable wettability alteration will be investigated for at least four distinct examples of crude oil/brine/rock/surfactant combinations.
The mechanism of increased recovery by manipulation of brine composition will be investigated for at least four crude oil/brine/rock combinations.

Addition of very low concentration surfactants to the imbibing aqueous phase will be explored as a means of increasing the rate of oil recovery by reducing the capillary forces which resist production of oil at the fracture face. At least twelve combinations of rock and fluid properties including both very strongly wetted and mixed wet rocks will be tested.

PROGRESS BY TASK - BUDGET PERIOD 1

Task 1. *Work of displacement and surface free energy.*

Introduction

Changes in surface areas between solid, oil and water take place during the process of displacement of oil from an oil reservoir. Multi phase flow and mass transfer are intricately related to the surface area between the three phases. Therefore for fundamental understanding of displacement, i.e. imbibition and drainage, the accompanying change in surface energy during these processes must be understood. Morrow (1970), measured changes in surface energy during drainage using thin section analysis for a packing of beads of uniform size. Epoxy resins of two different colors were used to simulate the wetting and the non-wetting phase. Indirect method of using interfacial tracer to determine the interfacial areas have been tried by a few researchers (Jain et al., 2003; Kim et al., 1997; Gladkikh et al., 2003). Bradford and Lei (1997) discuss theoretical ways of predicting changes in surface energy in soil samples.

The wetting state of the solid, i.e. oil-wet, water wet or mixed wet, has a significant impact on the interfacial areas and hence recovery from a particular reservoir. Bradford and Lei (1997), Jain et al. (2003), and, Gladkikh et al. (2003) discuss ways of altering the wettabilty of the sample by using different amounts of silanes. Bradford and Lei (1997) makes theoretical predictions for the changes in interfacial areas during imbibition and drainage whereas Jain et al. (2003) and Gladkikh et al. (2003) rely on the tracer technique to estimate the same quantities

In our research, actual core samples from outcrops are used for analysis. This involves a greater of degree of complication as compared to the work done by other researchers (Morrow, 1970, Jain et al., 2003, Kim et al., 1997, Gladkikh et al., 2003, Bradford and Lei, 1997, Scheafer et al., 2000a and 2000b) who worked with unconsolidated media (either bead pack or soil). Preliminary analysis will be done for Berea sandstone and a limestone sample. The experimental method is very similar to one discussed by Morrow (1970) that employs thin section analysis. In order to automate the process of analyzing an image obtained from the thin section, computer software is being developed. This will greatly reduce the time required for analysis.

Experimental

Theory of Stereology

Stereology is a science that provides us with a tool for calculating three dimensional information such as surface to volume ratio from a given two dimensional figure of the three dimension object. The various sampling probes that are commonly used are points, lines and planes. The fundamental relationships of stereology make no geometric assumption (Russ and Dehoff, 2000). The intersection of the probe with the image account for the geometric shape regardless of the way the body is embedded in the structure. However the values of these counts calculated from these interactions are then used to relate various geometric property of the body, such as surface to volume ratio, that are a defined as fundamental relationships. A detailed

analysis of the fundamental theorems, including proof and application is discussed by Underwood (1970) and Russ and Dehoff (2000).

Some fundamental theorems were applied to the data presented in this paper: For a particular phase, *a*, embedded in a second phase, *b*,

$$\langle P_a \rangle = A_a = V_a \qquad 1.1$$

Where, <> denotes that the equation is applicable to the average value of the population of the probe in 3 D space. P_a is the ratio of number of points lying in the phase *a* to the total number of points. A_a is the ratio of area occupied by phase *a* to the total area of the image. V_a is the ratio of volume occupied by the phase, *a*, to the total volume of the sample.

$$\langle L_a \rangle = 4 * V_a / S_a \qquad 1.2$$

Where, L_a is the mean intercept length of the phase *a*. V_a / S_a is the volume to surface ratio for the phase *a* in the image.

Using the above two relationships we obtain

$$S_v = (4/\langle L_a \rangle) * (P_a) \qquad 1.3$$

Where, S_v is the surface area of the phase *a* per unit volume of the sample.

For the present analysis there are three phases, wetting phase (blue), non-wetting phase (red) and solid (white). Since the above mentioned analysis is valid for two phases, we used a three step procedure to get the interfacial areas between the three phases. The procedure involved doing the line counts to get mean intercept length, which is then converted to interfacial surface areas using Eq. 1.3, of a particular phase while considering the other two phases as one phase. This generated three numbers that correspond to the mean intercept length of

- Red phase (non-wetting) and white (solid), S_R
- Blue phase (wetting) and white (solid), S_B
- White (solid) and liquid (red +blue), S_L

It is important to note that because there may be non-wetting and wetting phase (red-blue interface), the values of interfacial areas are calculated as

Interfacial area between red (non-wetting) and blue (wetting) phase, $S_{RB} = S_R + S_B - S_L$
Interfacial area between red (non-wetting) and white (solid) phase, $S_{RS} = S_R - S_{RB}$
Interfacial area between blue (wetting) and white (solid) phase, $S_{BS} = S_B - S_{RB}$

This method of analysis can be extended for the case in which there are *n* phases. In that case there will be *n* sets of equations and *n* variables that can be solved easily. Two additional quantities that are calculated are the total surface area and the created surface area.

Total surface area, $TSA = S_{RS} + S_{BS}$
Created surface area, $CSA = S_{RB} + S_{RS}$

Software - Theory

RGB approach

For every image that is created or stored on a computer the information, corresponding to the colors that are seen, is stored in the pixel format. Each pixel has three values corresponding to red, green and blue (RGB) and each of the three can have a value ranging from 0 to 255. All the colors seen in an image are a combination of RGB values between this range. The basic idea, while using this approach, was to read out the RGB value of each pixel one by one and identify whether it is red, blue or something else. The red color corresponds to the non-wetting phase, the blue is the wetting-phase and rest of the image is solid.

For the cases of a simple network model, drawn using any available commercial software similar to Adobe Photoshop, the size of the pixel and the values for RGB can be defined, for e.g. for red the RGB values are 255,0,0 and for blue 0,0,255. The software would then need to pick out, in a set of three, the value of RGB from the file containing the information about each pixel in the image. The format of this file is generally binary or ASCII.

HSV approach

Color can also be represented in the Hue/Saturation/Value (HSV) color model instead of the more standard Red/Green/Blue (RGB) model. The HSV color space is more intuitive to use and is much easier to divide into regions which correspond to perceptually recognized colors such as blue, green, pink etc. It is based on such intuitive color characteristics as tint, shade and tone (or family, purety and intensity). The coordinate system is cylindrical, and the colors are defined inside a hexcone. The hue value, H, ranges from 0 to 360 degrees. The saturation, S, is the degree of strength or purity and this ranges from 0 to 1. Purity is how much white is added to the color, so S=1 makes the purest color (no white). Brightness, V, ranges from 0 to 1, where 0 is black.

In order to use an image obtained from the microscope an intermediate processing step was needed because when an image of an actual sample was taken, it was found that the color of the epoxy (red or blue) varied from light to darker shades of their respective colors. In order to process this added complexity, the HSV approach is used to convert the raw image data in RGB format to HSV format to identify the variation in red and blue and also to pick out a range for other colors such as yellow, brown, purple etc.. Since the variation in red and blue in the raw picture varied between light pink to red for the non-wetting phase and purple to light blue to dark blue for wetting phase, these ranges of colors from the HSV format were used to generate the processed image that had only the type of pixels pure red (255,0,0), pure blue (0,0,255) and white (255,255,255). This processed file was then used for further analysis such as point counts and line counts.

Results and Discussion

Fig. 1.1 and 1.2 show the conversion of an original thin section image for Berea sandstone to the modified file containing only three colors i.e. red, blue, white. Further analysis of the picture including the accuracy of the computer generated image is being investigated. The next step will involve point and line counting to get saturations and interfacial surface areas using the fundamental equations of stereology.

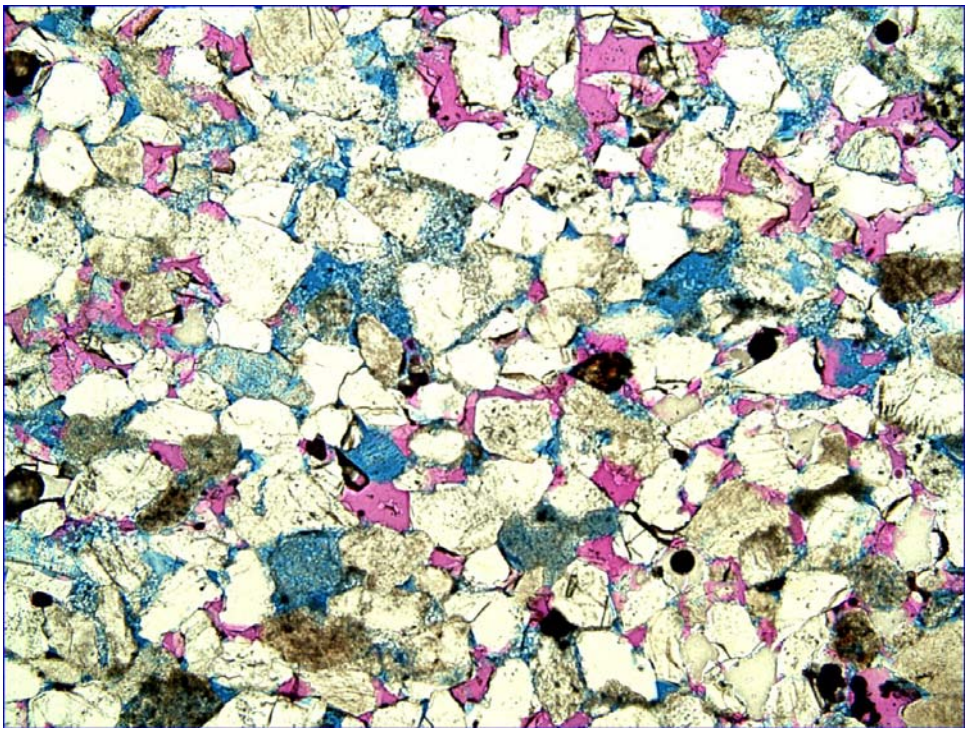

Fig. 1.1

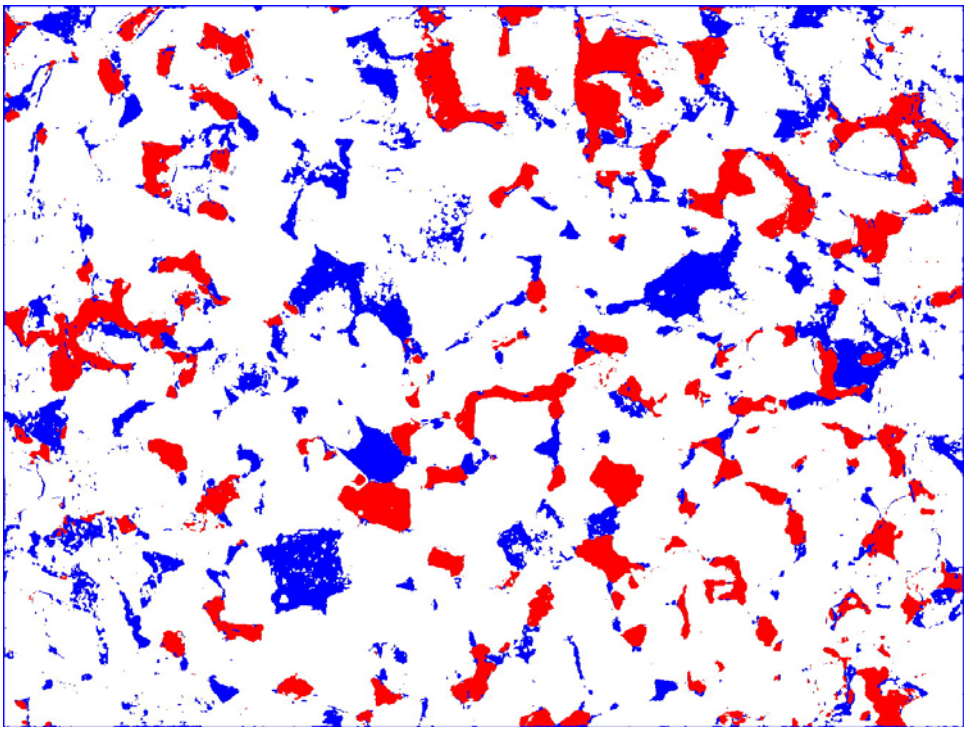

Fig. 1.2

Task 2. *Imbibition in simple laboratory and mathematical network models.*

Introduction

As observed in laboratory experiments, the rate of non-wetting phase (oil) recovery by spontaneous imbibition is strongly correlated with the viscosity ratio of the wetting phase (water) to non-wetting phase (oil). Analytical solutions of spontaneous imbibition in cylindrical capillary tubes have been derived, which reveal the dependency of the advancing position of the wetting phase to the viscosity ratio. The analytical solution in dimensionless format may lead to new understanding in scaling the recovery rates of laboratory experiments. One of the basic objectives of Task 2 is to use simple network models to investigate the time-lag phenomena during pressure build up in the non-wetting phase. The pressure build up in non-wetting phase, as observed in the imbibition by a one end open core, is closely related to the capillary back-pressure that opposes production of the non-wetting phase at the outflow face. At the pore scale, the complexity of the boundary conditions at the interfaces between fluids and between the fluids and the solid rock matrix means that an exact mathematical description is often difficult to obtain for all but the simplest cases. Moreover, the fluid motion at the three-phase contact line between moving immiscible fluids and a solid boundary is still not completely understood. Nevertheless it is possible to predict the fluid flow in several idealized pore geometries, such as through cylindrical tubes. In spontaneous imbibition, capillary pressure is considered as the dominant driving force, where the Poiseuille region covers practically the whole of the flow. Based on the Poiseuille's law, spontaneous imbibition models for water replacing oil and water replacing gas in simple pore units have been derived. Accordingly, numerical solving schemes and computer codes have been developed. This is the first step toward to large scale network models for imbibition.

Experimental

Spontaneous imbibition in cylindrical capillary tubes

The behavior of spontaneous imbibition in a cylindrical capillary tube, as shown in Figure 2.1, is determined by two factors, the capillary pressure and the viscosity ratio of the wetting phase (water) to non-wetting phase (oil).

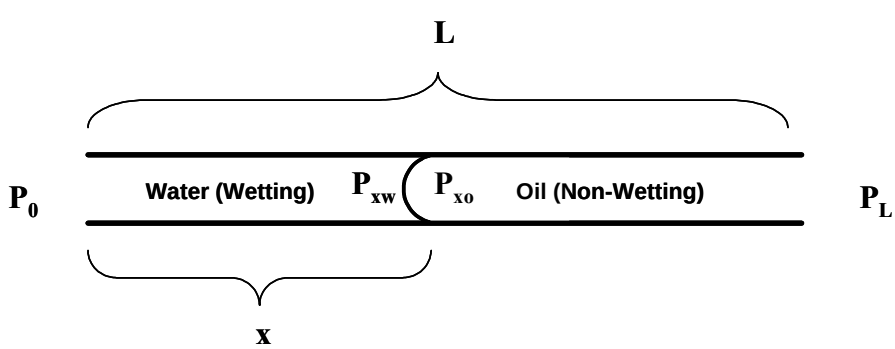

Figure 2.1. The advancing meniscus of water phase in a cylindrical capillary tube by spontaneous imbibition.

In Figure 1, P_{xw} and P_{xo} are the pressures of the water phase and oil phase at the advancing meniscus, respectively. Therefore, the capillary pressure, P_c, is the difference between P_{xw} and P_{xo}.

$$P_c = \frac{2\sigma\cos\theta}{r} = P_{xo} - P_{xw} \tag{2.1}$$

When the water-oil interface advances to x, the water and oil flow rates can be calculated from the Poiseuille's law.

$$q_w = \frac{\pi(P_0 - P_{xw})r^4}{8\mu_w x} \tag{2.2}$$

$$q_o = \frac{\pi(P_{xo} - P_L)r^4}{8\mu_o(L-x)} \tag{2.3}$$

Considering water and oil as incompressible fluids, we have $q_w = q_o$

So $$\frac{P_0 - P_{xw}}{\mu_w x} = \frac{P_{xo} - P_L}{\mu_o(L-x)} \tag{2.4}$$

In case, the capillary pressure is the only driving force, we assume that there is no pressure difference at the two tube ends, i.e.

$$P_0 = P_L \tag{2.5}$$

From Eq. (2.1)~(2.5), we obtain the water flow rate as

$$q_w = \frac{\pi P_c r^4}{8[\mu_o(L-x) + \mu_w x]} \tag{2.6}$$

When the water-oil interface is at x, the flow volume balance is described by the following differential equation,

$$dV = \pi r^2 dx = q_w dt \tag{2.7}$$

Solving (2.6) and (2.7) by integration, we obtain an analytical solution, Eq. 2.8, of spontaneous imbibition in cylindrical capillary tubes.

$$(\mu_o - \mu_w)x^2 - \mu_o L x + \frac{P_c r^2}{4} t = 0 \tag{2.8}$$

This solution is consistent with the results from Washburn (1921) and Morrow and Mason (2001) on three special cases, μ_o=0, μ_w=0, and μ_o= μ_w. When μ_o=0, such as water displacing gas, Eq. 2.8 becomes Eq. 2.9.

$$\left(\frac{x}{L}\right)^2 = \frac{rt\sigma\cos\theta}{2\mu_w L^2} \tag{2.9}$$

When μ_w=0, such as gas displacing oil, Eq. 2.8 becomes Eq. 2.10.

$$1-(1-\frac{x}{L})^2 = w \tag{2.10}$$

where $w = \frac{rt\sigma\cos\theta}{2\mu_o L^2}$.

When μ_o= μ_w, Eq. 2.8 becomes Eq. 2.11.

$$\frac{x}{L} = \frac{w}{2} \tag{2.11}$$

In general, if $\mu_o \neq 0$, the solution of Eq. 2.8 can be given as

$$\frac{x}{L} = \frac{w}{1+\sqrt{1-(1-\frac{\mu_w}{\mu_o})w}} \tag{2.12}$$

As shown in Figure 2.2, where the capillary pressure is fixed, the rate of invading water varies significantly with different viscosity ratios of the wetting phase (water) to non-wetting phase (oil). This result could lead to new understanding in scaling the recovery rates of laboratory experiments.

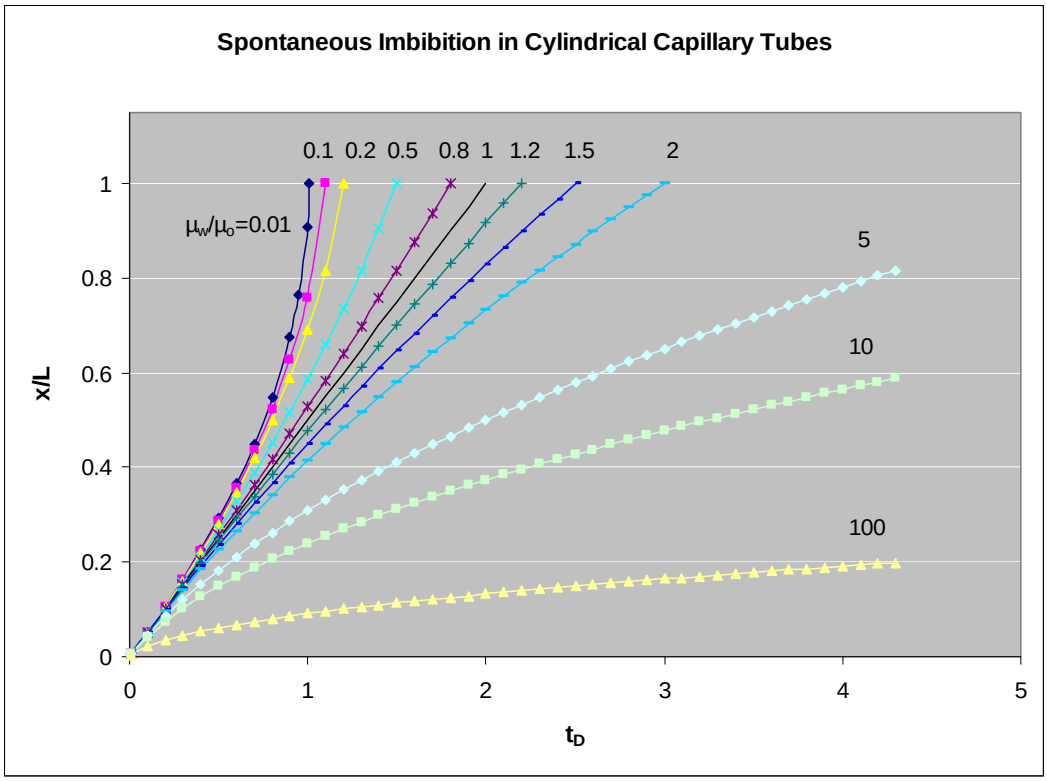

Figure 2.2. The effect of viscosity ratio on spontaneous imbibition in cylindrical capillary tubes.

Results and Discussion

Water-oil spontaneous imbibition in "Hub and Spoke Units"

To simulate the time-lag phenomena during pressure build up in the non-wetting phase, we consider a simple network model consisting of a number of pore units, named as "Hub and Spoke Units". Each Unit consists of a sphere and several connecting cylindrical tubes as illustrated in Figure 2.3. Every tube of a Unit can be classified by one of three possible cases: end opens to the network boundary; end is a closed end; or end is connected (shared) with another Hub and Spoke Unit.

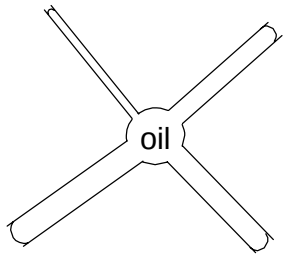

Figure 2.3. A Hub and Spoke Unit with four open-ended tubes.

To demonstrate how spontaneous imbibition is simulated in such network models, we consider the simplest network model that has only one Unit. For generality, we assume that the Unit has n tubes with the radii of $r_1 \le r_2 \le \cdots \le r_n$. All tubes are open to the network boundary

and that the hub in the following analysis has no volume. Other variables are defined in following:

Outside network pressure: P
Pressure inside the sphere of the Hub and Spoke Unit: $p(t)$ at any given time t
The unit of length measurement: L
The lengths of tubes: $L_1, L_2, \cdots, L_n$
The invading water front position in tubes: $x_1, x_2, \cdots, x_n$ at any given time t

To make the analysis applicable to general cases, dimensionless variables are used for the network model. We first define two parameters, a and b, and a dimensionless time unit t_D as

$$a = \frac{2\sigma\cos\theta}{PL} \text{ and } b = \frac{P}{8\mu_w} \tag{2.13}$$

$$t_D = bt \tag{2.14}$$

The dimensionless radius, length, invading position are defined by

$$r_i^* = \frac{r_i}{L}, L_i^* = \frac{L_i}{L}, x_i^* = \frac{x_i}{L}, i = 1 \sim n \tag{2.15}$$

The dimensionless pressure inside the sphere of the Hub and Spoke Unit is defined by

$$p^*(t) = \frac{p(t)}{P} \tag{2.16}$$

Similarly, the dimensionless capillary pressure in tube i is defined by

$$p_{ci}^* = \frac{p_{ci}}{P} = \frac{a}{r_i^*} = p_{io}^* - p_{iw}^* \tag{2.17}$$

In Eq. 2.18, the redefined water and oil flow rates are not dimensionless but have a unit of *1/t*. However, the time unit will be eliminated in the final differential equation of Eq. 2.21.

$$q_{iw}^* = \frac{q_{iw}}{L^3}, q_{io}^* = \frac{q_{io}}{L^3} \tag{2.18}$$

Therefore, the Poiseuille's law of Eq. (2.2) and (2.3) for the tubes of the Hub and Spoke Unit can be rewritten as Eq. (2.19) and (2.20)

$$q_{iw}^* = \frac{\pi(1 - p_{iw}^*)(r_i^*)^4}{x_i^*} b \tag{2.19}$$

$$q_{io}^* = \frac{\pi(p_{io}^* - p^*(t))(r_i^*)^4}{L_i^* - x_i^*} (\frac{\mu_w}{\mu_o}) b \tag{2.20}$$

$$i = 1, 2, \cdots n$$

Similar to Eq. 7, the flow volume balance in each tube is described by a differential equation of

$$\pi(r_i^*)^2 dx_i^* = q_{iw}^* \frac{dt_D}{b} \quad \text{and} \quad q_{io}^* = q_{iw}^* \tag{2.21}$$
$$i = 1,2,\cdots n$$

The spontaneous imbibition procedure of a single Hub and Spoke Unit is therefore governed by Eq. 2.19~2.21. For most cases, it will be no easy to find an analytical solution of Eq. 2.19~2.21 but they can be solved numerically. A numerical method is provided in the next section, where the spontaneous imbibition of water displacing gas is discussed. A similar, but simpler, numerical solving procedure can also be applied to the spontaneous imbibition of water displacing oil.

Water-gas spontaneous imbibition in "Hub and Spoke Units"

The same Hub and Spoke Unit model and conditions as described above are assumed in this section except the Unit is initially saturated with gas instead of oil. Here, the gas viscosity is negligible. When the gas inside the Unit is compressed by invading water, the gas obeys the Boyle's Law: for a given mass, at constant temperature, the pressure times the volume is a constant.

$$pV = mRT \tag{2.22}$$

where p is the gas pressure, V is the gas volume, T is temperature, m is the number of moles, and R is the constant value for each gas. For air, R=0.286 kj/kg/K^o.

Let V^0 and V^t represent the initial gas volume and the gas volume at time t. We have

$$V^0 = \sum_i \pi L_i r_i^2, \quad V^t = \sum_i \pi (L_i - x_i^t) r_i^2 \tag{2.23}$$

or in the dimensionless format

$$V^{*0} = \frac{V^0}{L^3} = \sum_i \pi L_i^* r_i^{*2}, \quad V^{*t} = \frac{V^t}{L^3} = \sum_i \pi (L_i^* - x_i^{*t}) r_i^{*2} \tag{2.24}$$
$$i = 1,2,\cdots n$$

According to the Boyle's Law of Eq. 2.22, we obtain

$$p^*(t_D) = \frac{p^{*0} V^{*0}}{V^{*t_D}} \tag{2.25}$$

In addition, because gas pressure is the same everywhere inside the Hub and Spoke Unit, the Poiseuille's law of Eq. 2.19 becomes

$$q_{iw}^* = \frac{\pi(1 - (p^*(t_D) - p_{ci}^*)) r_i^{*4}}{8\mu_w x_i^t} \tag{2.26}$$

The equations of Eq. 2.21, 2.24, 2.25, and 2.26 form the mathematical model for the water-gas spontaneous imbibition in a Hub and Spoke Unit. A numerical scheme has been developed to solve the proposed mathematical model. The procedure is briefly described in below.

Suppose we have obtained the advancing/retreating positions in each tube, $x_i^{*t_D}, i = 1 \sim n$, at time t_D. For a given time increment Δt_D, we want to calculate $x_i^{*t_D+\Delta t_D}, i = 1 \sim n$. The computation can be summarized by three steps:

(1) Knowing $x_i^{*t_D}$, $p^*(t_D), i = 1 \sim n$

(2) Calculating $x_i^{*t_D+\Delta t_D}, i = 1 \sim n$ from Eq. 2.21 and 2.26, precisely,

If $(1-(p^*(t_D)-p_{ci}^*)) \geq 0$ then $x_i^{*t_D+\Delta t_D} = \sqrt{(x_i^{*t_D})^2 + 2(1-p^*(t_D)+p_{ci}^*)(r_i^*)^2 \Delta t_D}$

If $(1-(p^*(t_D)-p_{ci}^*)) < 0$ then $x_i^{*t_D+\Delta t_D} = 2x_i^{*t_D} - \sqrt{(x_i^{*t_D})^2 - 2(1-p^*(t_D)+p_{ci}^*)(r_i^*)^2 \Delta t_D}$

(3) Updating $p^*(t_D)$ from Eq. 24 and 25.

Repeating the above three steps for each time increment until the spontaneous imbibition process is completed. Various cases of Hub and Spoke Unit settings will be simulated to investigate the time-lag behavior during pressure build up in the gas phase. The results will be reported in the next quarterly.

Task 3. *Novel observations on fluid pressures during imbibition and the mechanism of non-wetting phase production at the imbibition face.*

Introduction

Saturation profiles

The simulation showed the conditions under which the frontal wetting phase saturations are finite. The measured WP saturations of both water/oil and oil/air imbibition when the front arrives at the dead end boundary were between 0.38 and 0.46 for the 8 samples. The final saturation for both water/oil and oil/air imbibition are between 0.43 and 0.53 for all tested samples. The development of the simulated saturation profiles as the front travels through the core is illustrated in Fig. 3.1. The frontal WP saturations for both oil/air and water/oil imbibition were between 0.25 and 0.345 for the simulations for all tested samples. Because of the similarity solution, the profiles in the frontal flow period can be collapsed into a single curve by normalization with respect to distance advanced. The saturations in the post contact period rise globally and eventually reach saturation, S_{w0},

The simulated saturation profiles for water/oil are more curved at both the front and the end than for oil/air. This reflects the lower mean transmissibility at the front and at the exit end of the profile for flow of the more viscous nonwetting phase (oil).

It is noted that, even though the viscosity of air is lower than water and the oil is 3.8 cp in both water/oil and oil/air cases, the frontal period flow rate in the water/oil case is about three times faster than the flow rate in the oil/air case for the same recovery. An important contributing factor to this difference is that the interfacial tension of water/oil is almost twice that for oil/air. Also the viscosity of the WP in the oil/air case is 3.8 time the viscosity of the WP in the water/oil

case. Because relative permeability for the WP in Berea sandstone is much lower than relative permeability for the non-wetting phase in a large part of the transitional profile, both interfacial tension and WP viscosity will tend to decrease WP (oil) flow in the oil/air case.

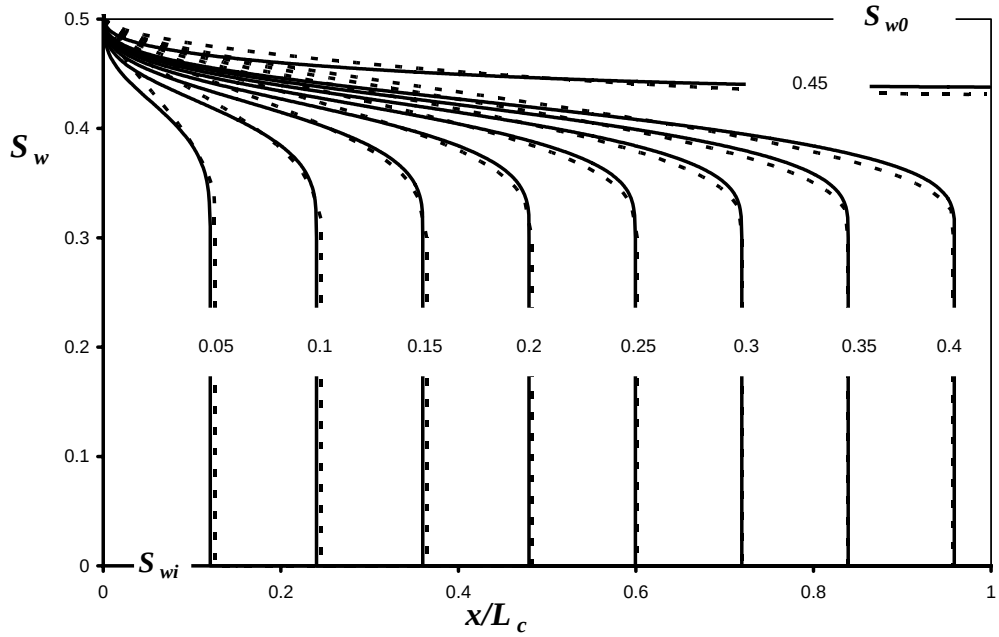

Fig.3.1 Simulated saturation profiles during water/oil COUCSI for Core H8O (solid lines) and oil/air COUCSI for core H8A (dashed lines). The intervals of the recovery, Q_w/V_ϕ are 0.05.

Pressure profiles

As imbibition progresses, the pressure profiles stretch over an increasing distance from the core inlet as shown in Fig. 3.2 for water/oil and in Fig. 3.3 for oil/air. The value of capillary back pressure, P_{cb}, is equal to the difference between $P_{end,}$ measured during the frontal flow period, and the pressure drop in the NWP that drives the viscous flow. For imbibition of brine against 0.0038 *Pa.s* oil, the value of P_{cb} was 1.3 *kPa* in the 1.094 μm^2 Berea sandstone core. The measured P_{end} during the frontal flow period was 3.140 *kPa*. For the oil/air results, from the enlarged simulated distribution of the NWP pressure shown in Fig. 3.3, it can be seen that the behavior of P_{nw} in the oil/air case is comparable to that in the water/oil case. However, P_{end} is only 0.038 *kPa* higher than P_{cb}. This difference can be neglected for most practical purposes.

The overall character of the pressure behavior can be expected from the similarity solution. The solution infers that for the advance of any particular saturation, S_w, along the core, the difference between its associated capillary pressure and the back capillary pressure ($P_c(S_w) - P_{cb}$) is constant until the front contacts the closed end of the core.

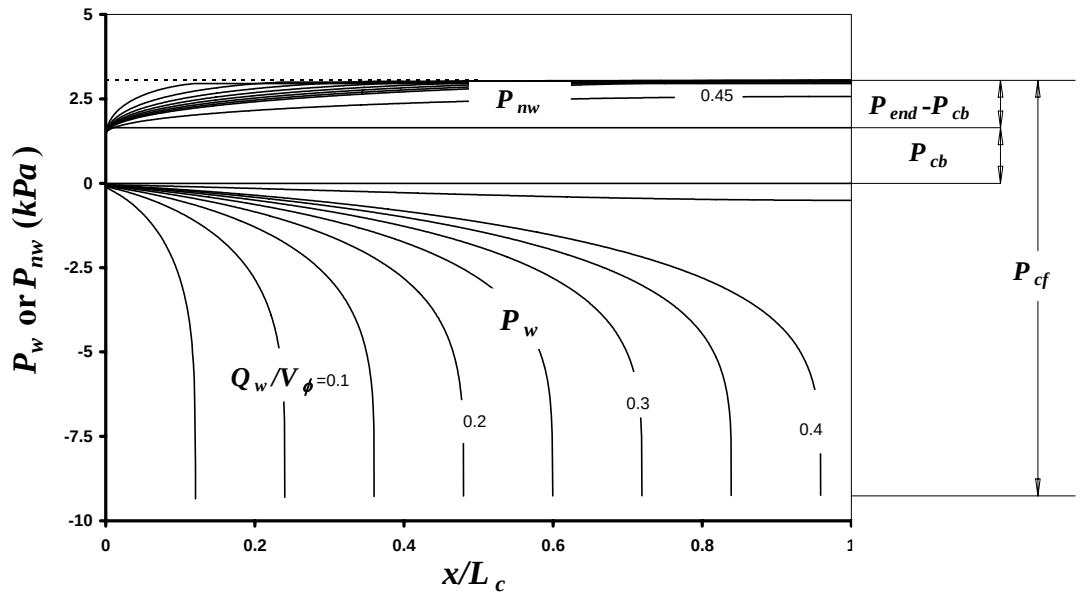

Fig.3.2 Pressures profiles of WP and NWP during water/oil COUCSI in Core H8O determined by simulation. The maximum difference between P_{nw} and P_w is equal to the capillary pressure, P_{cf}, at the front (the value is 12.359 *kPa*).

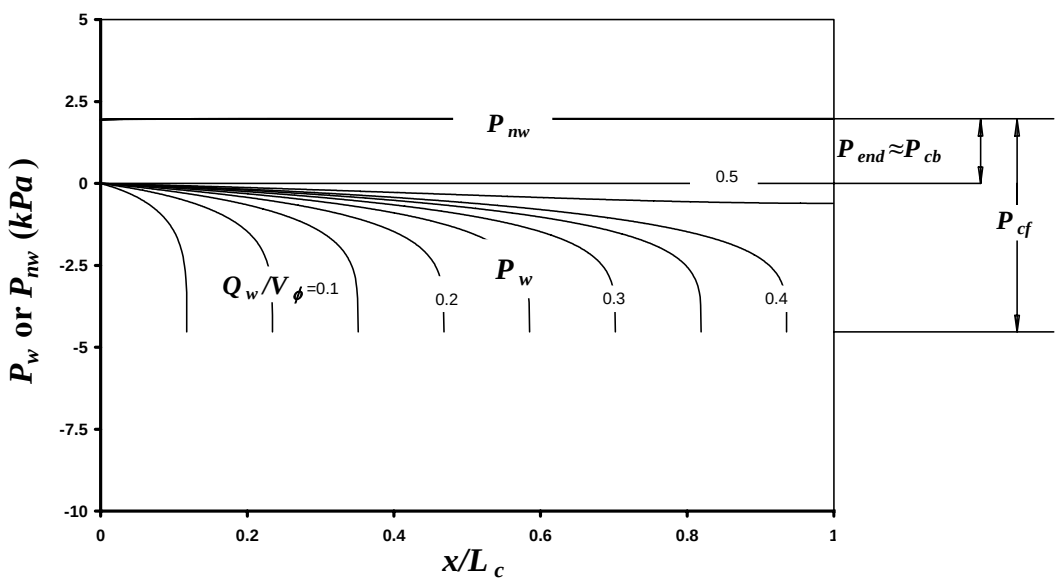

Fig.3.3 Pressures profiles in WP and NWP during oil/air COUCSI in Core H8A determined by simulation. The maximum difference between P_{nw} and P_w is equal to the capillary pressure at the front,

P_{cf}, (the value is 6.500 *kPa*). For oil/air, the difference between the end pressure, P_{end}, and back capillary pressure, P_{cb}, is hard to distinguish at the scale of the diagram.

Experimental

COUCSI displacement curvatures

The frontal capillary pressures, P_{cf}, during COUCSI was measured directly by experiment for the highest permeability Berea. The principle of the method is that if the frontal capillary pressure, P_{cf}, is lower than the capillary back pressure, P_{cb}, COUCSI will stop and the transducer will indicate the frontal capillary pressure. This was achieved by butting a slice of low permeability core at the face of the high permeability core. Imbibition was initially made co-current by temporarily opening the connection to the pressure transducer. After the front had entered the high permeability core, the pressure transducer was reconnected. Movement of the imbibition front eventually stopped because the capillary pressure at the front in the high permeability core was less than P_{cb} for the low permeability end piece. The estimate of P_{cf} in cores with permeability of about 1.05 μm^2 for both water/oil or oil/air cases was obtained from the increase in end pressure. The frontal interface curvatures (P_c/σ) were the same (0.254 μm^{-1}) for both water/oil and oil/air imbibition. This observation is consistent with the assumption that very strongly wetted conditions pertained for both water/oil and oil/air imbibition.

Table 3.1. Conditions for measurement capillary pressures at the imbibition front.

COUCSI	OIL/WATER	AIR/OIL
μ_{nw}/μ_w	0.0038 *Pa.s*/0.00102 *Pa.s*3.7255	0.000018 *Pa.s*/0.0038 *Pa.s*
σ	48.85mN/m	25.87mN/m
CORE	H6O	H5A
d(cm)	3.795	3.79
L(cm)	6.967	8.04
K(μm^2)	1.067	1.042
ϕ	0.222	0.221
P_{cf}(*kPa*)	12.359	6.600
P_{cf}/σ μm^{-1}	0.253	0.255

Simulations were performed for water/oil COUCSI in core H8O and for oil/air COUCSI in H8A (Figs. 3.4 and 3.5). The permeabilities of both cores were about 1.05 μm^2. If the relative permeabilities are similar and capillary pressures are scaled for the Berea sandstones, the pair of P_{cf} and P_{cb} for any core can be found by running the simulations until the three experimental curves prior to FAB were matched. For self similar displacement, many saturation profiles can give the same performance prior to FAB. In general, however, they do not have the same post FAB performance. Information about profiles, therefore, can only be derived from post FAB performance.

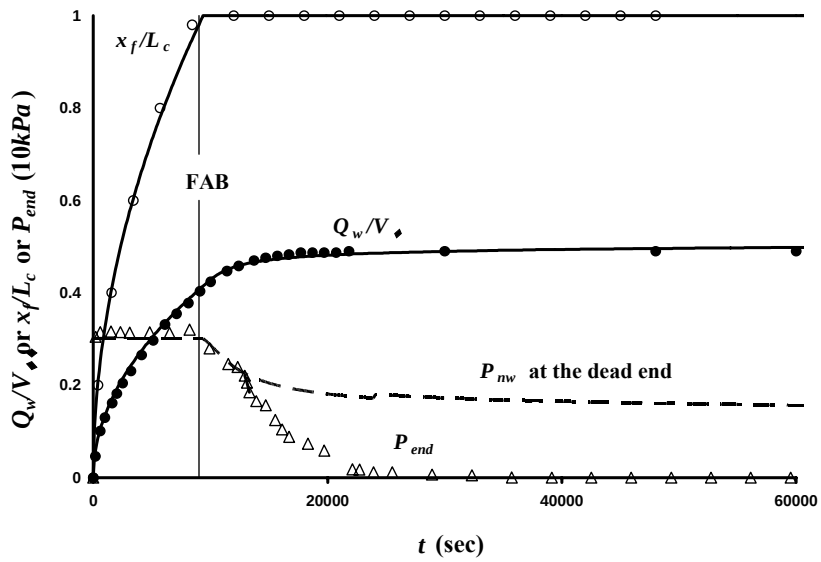

Fig.3.4: Comparison of experimental and simulated results for imbibition of brine against oil (Core H8O). The points are the experimental data; the continuous lines are from simulations.

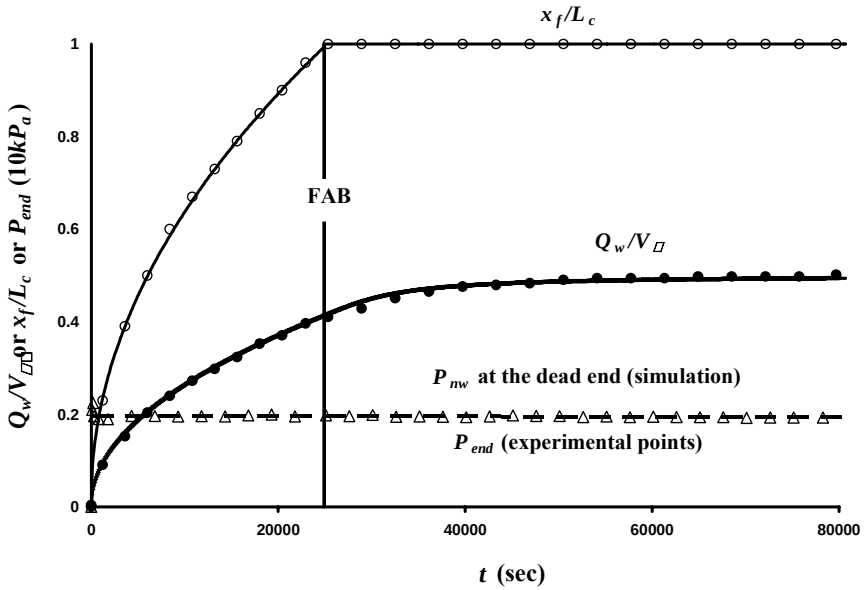

Fig.3.5. Comparison of experimental and simulated results for imbibition of oil against air (Core H8A). The points are the experimental data; the continuous lines are from simulation.

The values of P_{cf} and P_{cb} in water/oil and oil/air cases for different permeability Berea sandstone are listed in Table 2. The P_{cb} in the oil/air cases is almost equal to P_{end} in the frontal flow period because resistance to flow of the very low viscosity NWP (air) is very small. For water/oil imbibition, P_{cb} is significantly lower than P_{end} in the frontal flow period because of the viscous resistance to flow of the non-wetting phase liquid.

Results and Discussion

Comparison of water/oil and oil/air capillary displacement mechanisms can be made in terms of effective radii given respectively by capillary pressure and permeability. Porous media can be characterized by the radius of an equivalent parallel bundle of equal tubes model (the Leverett microscopic pore radius), $r_L = \sqrt{\frac{8K}{\phi}}$. Capillary pressure is also related to some characteristic radius given by $2\sigma/P_c$. Plots of the interface radii versus the Leverett radii are presented in Fig. 3.6. Both radii increase together as expected. Curvatures at the displacement front, C_f ($=P_{cf}/\sigma$), for a given core are the same for both water/oil and oil/air imbibition (see Fig. 10). The radii at the open face, r_b, associated with the capillary back pressure, P_{cb}, are much lower for production of oil (water/oil imbibition) than for production of air (oil/air imbibition). This is probably due to the differences in conditions at the onset of production. For imbibition of water against oil, oil is produced almost instantaneously after immersion in brine. For imbibition of oil against air, because of the compression period, production of air bubbles is delayed. As oil invades the core, oil/air interfaces drive into the core building up the air pressure. Eventually, the air passes through a series of pore throats and accesses the open face. The selectivity of gaining the path by which gas is produced explains why gas bubbles are produced from only one or two locations on the open face. In contrast, oil bubbles appear almost instantaneously at many points on the open face. The scaled capillary curvature, C_b ($=P_{cb}/\sigma$), associated with back pressure at the open face in the oil/air case range from about 2/5 down to 1/3 of the interface curvature at the front, C_f. For water/oil COUCSI the ratio of C_b ranges from about 1/4 down to 1/9 of C_f. Thus the contribution to the relative reduction in rate of flow of the NWP because of the capillary back pressure at the open face for oil/air imbibition is about 2.4 to 3 times that for water/oil imbibition.

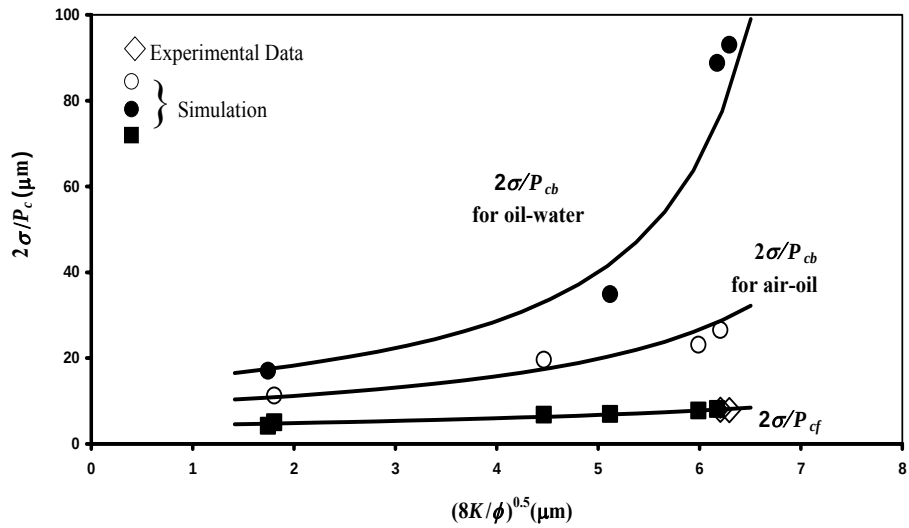

Fig. 3.6 Relationships between meniscus radii at the front and at the open face compared with the Leverett radius. Solid circles represent the water/oil data ($\sigma_{o\text{-}w}$ = 48.85 *mN/m*) and open circles the oil/air data ($\sigma_{a\text{-}o}$ = 25.87 *mN/m*).

Task 4. *Network/numerical model and new imbibition data.*

Introduction

A third set of imbibiton data was obtained for the mineral oil of 43 cp viscosity. As for the previous sets, the desired oil phase viscosity was prepared by mixing low viscosity oil and high viscosity oil. Mineral oil properties were included in the previous quarterly. As in the foregoing experiments, glycerol was used as the aqueous phase viscosifying agent. Additional data of oil recovery at very strongly water-wet conditions was obtained for a constant oil phase viscosity of 43 cp and aqueous phase viscosities ranging from 1-1650 cP. The results showed comparable characteristics to data set NM(22). The imbibition curves were closely correlated for the lower aqueous phase viscosity tests. As for the previous results, NM(4) (μ_o= 4 cp) and NM(22) (μ_o= 22 cp) an increase of the viscosity ratios was accompanied by increase of the final oil recoveries up to a viscosity ratio of about 4. The residual oil was about 52.5 % at higher viscosity ratios.

Experimental

MATERIALS

For all tests in this experimental set the same liquids and sandstone cores as used in sets NM(4) and NM(22) were utilized. Also, the preparation steps were identical to the aforementioned experimental sets.

Fluid flow was 3-dimensional as a result of the all faces open boundary condition for each core. Hence the characteristic length, L_c, for each core is defined by (Zhang et al., 1996)

$$L_C = \frac{ld}{2\sqrt{d^2 + 2l^2}} \tag{4.1}$$

and was close to 1.24 cm for each core as a result of the identical size and geometry. Oil production as a function of time was measured in standard imbibition cells at ambient temperature and with 0% initial water saturation for each test.

Results and Discussion

As for the preceding sets the modified Ma et al. scaling group was applied to correlate the results for this experimental set with the oil phase viscosity fixed at 43 cp .

$$t_D = t * \sqrt{\frac{k}{\phi}} * \frac{\sigma}{\mu_g} * \frac{1}{L_c^2} \tag{4.2}$$

SPONTANEOUS IMBIBITION

Cores and fluid properties for this non-matched viscosity experimental set termed as NM(43) are listed in Table 4.1. Cores cut from the same block of sandstone had permeability and porosity that was consistently of about 67 md and 17 % respectively. Two of the total of nine cores, namely C5-21 and C5-17, were cut from a higher permeability Berea sandstone block and had somewhat higher than average permeability and porosity. The aqueous phase viscosity exhibited slightly higher than average permeability and porosity. The aqueous phase viscosity ranged from 1.1 cp for seawater to 1646.6 cp for glycerol.

Table 4.1 Rock and Aqueous Phase Properties
NM(43): μ_o= 43 cP, ρ_o= 0.843 g/cm^3

Core #	L_c cm	k_g md	Φ %	σ_{ow} dyn/cm	ρ_{ap} g/cm^3	μ_{ap} cP
C1-11	1.237	68.7	17.1	53.1	1.024	1.1
C1-12	1.242	62.5	17.2	41.7	1.121	4.4
C1-13	1.238	55.6	16.7	36.4	1.172	15.2
C1-15	1.241	70.4	17.2	34.6	1.197	35.4
C1-14	1.240	70.0	17.2	32.4	1.220	96.6
C5-21	1.234	82.0	18.2	31.9	1.222	99.9
C1-19	1.237	69.9	16.8	31.1	1.237	228.4
C5-17	1.236	77.2	18.0	29.6	1.249	522.7
C1-18	1.236	67.4	16.2	28.5	1.262	1646.6

Results for Set NM(43) are illustrated in Fig. 4.1. Except for core C5-17 being somewhat out of sequence, comparable characteristics to Set NM(22) were observed. Close correlation was obtained for the lower μ_{ap} tests (up to 99.9 cP), but as for Set NM(4) and Set NM(22), there was still a slight systematic increase in t_D with μ_{ap}. The dimensionless times increased as μ_{ap} increased at higher μ_{ap}, and as for data set NM(22), became stretched with increase in recovery. Final oil recoveries increased slightly with increase in viscosity ratio up to a viscosity ratio of about 4. The residual oil was close to constant at 52.5 % ± ½ at higher VR.

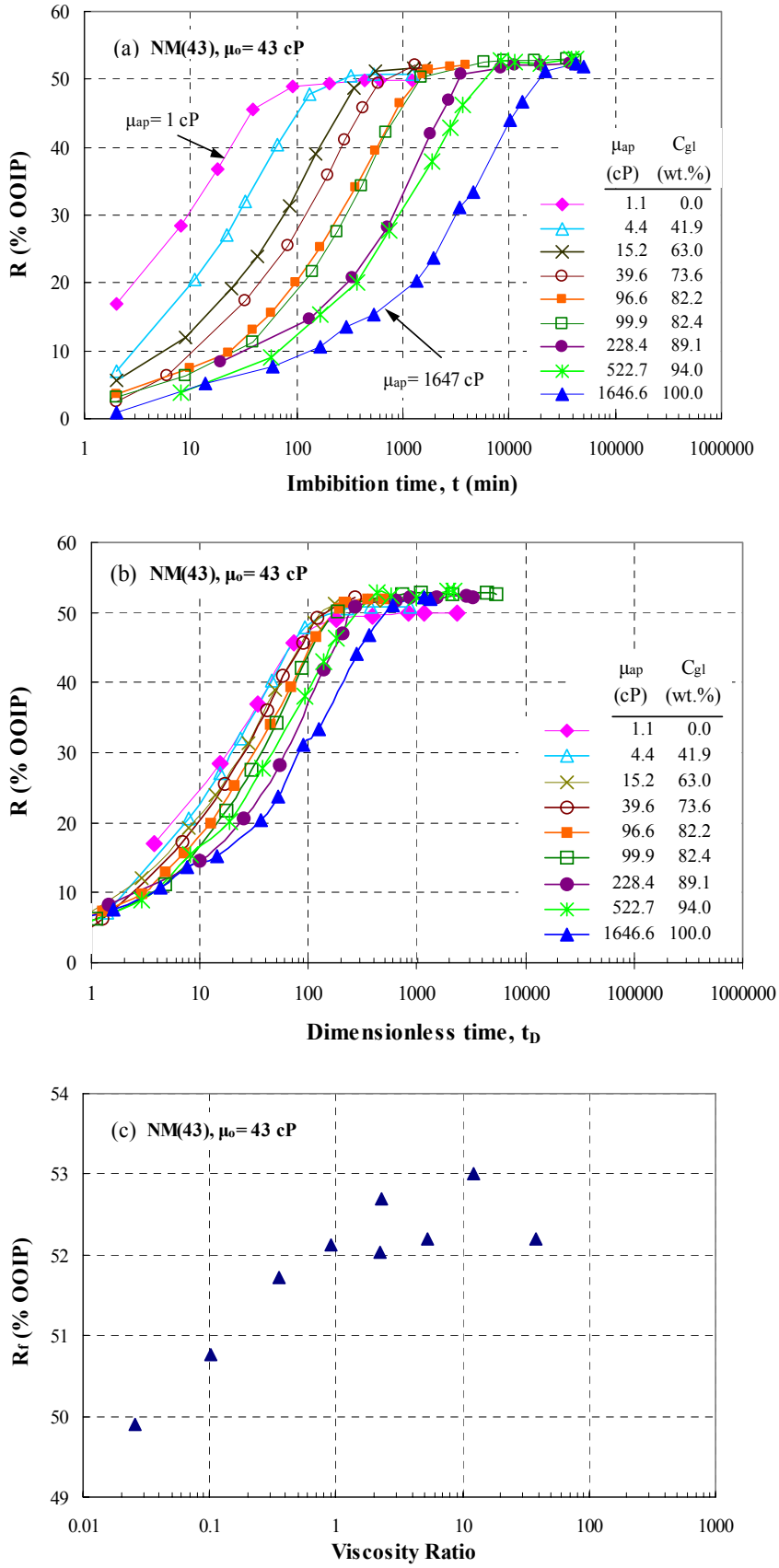

Fig. 4.1. Recovery of 43 cP oil by spontaneous imbibition for variation in aqueous phase viscosity versus (a) time (b) dimensionless time; (c) final oil recovery, R_f, versus viscosity ratio.

Plots of time versus viscosity ratio as well as dimensionless time versus viscosity ratio with normalized recovery as parameter are shown in Fig. 4.2. Relationships between dimensionless time and viscosity ratio are closely comparable to those given by Set NM(22). The recovery curves show only slight increase in t_D with increase in VR up to 4 and marked systematic increase at higher values of VR.

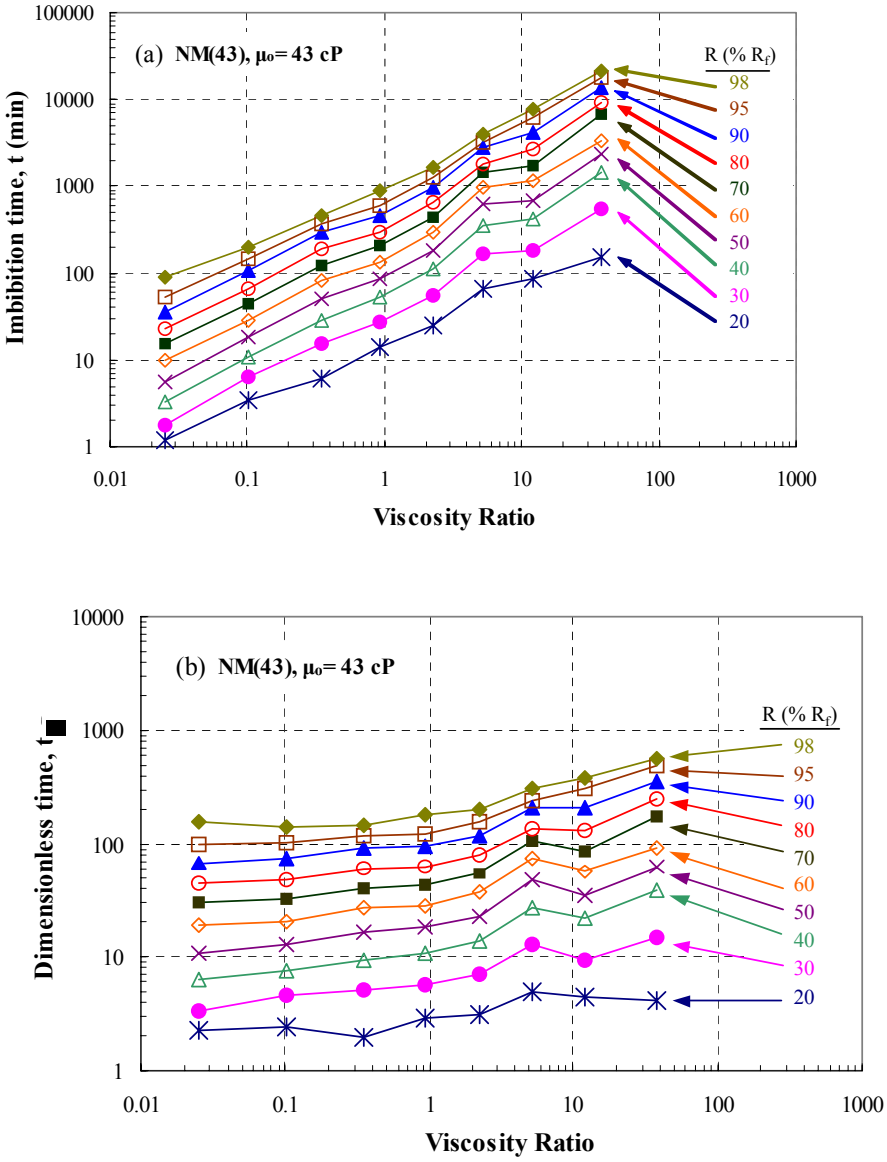

Fig. 4.2. Imbibition time (a) and dimensionless time (b) versus viscosity ratio (μ_o = 43 cP) for fractional recoveries, R, ranging from 20 % to 98 % (interpolated values for individual cores).

The conclusion for this experimental set is similar to Set NM(4) and Set NM(22). Results of spontaneous imbibition with low aqueous phase viscosities (and thus low viscosity ratios) could be correlated closely. As the viscosity ratio increased, the dimensionless time increased distinctly too. In the low viscosity ratio range the final oil recovery increased as the viscosity ratio increased. At higher viscosity ratios the final oil recovery remained about constant.

Task 5. *Comparison with similarity solutions.*

Introduction

The objective of Task 5 is to compare results given by simulation with special case analytic results given by similarity solutions for spontaneous imbibition for at least five distinct cases of rock and fluid properties. From the analysis given in the third quarterly report and the solution for pressure distribution in the previous report; the verification follows.

Verification

The analytical solutions were verified by comparison with numerical simulations which represent approximate solutions to the same equations. These simulations used an explicit, two-phase simulator. The operation of the simulator is described in Ruth et al. (2000). In that paper it was shown that spontaneous imbibition can be modeled using numerical simulation, and a set of relative permeability and capillary pressure curves were developed that allowed prediction of experimental data.

The curves used are of the form

$$k_{ro} = k_{roe}\left(\frac{S_{wo} - S_w}{1 - S_{wo}}\right)^{n_o} \tag{5.1}$$

$$k_{rw} = k_{rwe}\left(\frac{S_w}{1 - S_{wo}}\right)^{n_w} \tag{5.2}$$

and

$$P_c = P_{ct}\left[1 - B\ln\left(\frac{S_{wo} - S_w}{1 - S_{wo}}\right)\right] \tag{5.3}$$

Here S_w is the water saturation. S_{wo} is the saturation at the open face (which corresponds to the final saturation at the end of counter-current spontaneous imbibition). The endpoint relative permeabilities are denoted by k_{roe} and k_{rwe} while n_o and n_w are exponents that control the shapes of the curves. The final counter-current spontaneous imbibition saturation, S_{wo}, is always lower than the final co-current spontaneous imbibition saturation or the final forced imbibition saturation, (1-S_{or}) (see Li et al., 2003). S_{or} is the residual oil saturation, the saturation when the remaining oil is discontinuous in the porous media. For the capillary pressure (P_c) curve during counter-current spontaneous imbibition, P_{ct} is the capillary pressure at S_{wo}. B is a scale parameter. The values of the test parameters are given in Table 5.1. These properties were chosen to illustrate the method; however, the conclusions of this paper are general and not dependent on any particular values of the test parameter. The values of the saturation at the open face and the front can be determined experimentally. (Although they might be determined from basic principles, a procedure to achieve this has not yet been discovered. The conclusions of the present paper do not depend on the particular values of these saturations. The experimental values of these saturations will be the subject of future study.)

A number of cases were studied. First, the case of imbibition into a sample initially fully saturated with oil was analyzed. This was done in two ways. First it was assumed that both the initial water saturation and water saturation at the front are zero. The results are shown in Fig. 5.1. Fig. 5.1a contains the relative permeability and capillary pressure curves (all curves used in the present study are part of those shown in this figure). Fig.5.1b shows the saturation profile at an arbitrary time (in this case 30 s). Results for the analytical solution are shown by a solid line; the simulation results are shown by open circles. The agreement is excellent. Fig. 5.1c shows the production as a fraction of the pore volume Q_w / V_ϕ, the volume swept by the wetting phase, V_w / V_ϕ (which is equal to the position of the front as a fraction of the sample length, $x_f(t)/L$), and the pressure of the oil at the front, P_{of}. Again the agreement is excellent. The time at which the front reaches the end of the sample is denoted by 'fab'; the validity of the similarity solution ends here. Note that the pressure of the oil at the front is a constant as predicted by the theory. Fig. 5.1d shows the pressure profiles in the two phases based on the curves given in Fig. 5.1b. Again agreement is excellent.

Table 5.1: The Test Parameters

Variable	Value	Units	Variable	Value	Units
ϕ	0.215	-	k	600.0	mD
L	6.00	cm	D	3.18	cm
μ_o	2.00	cp	μ_w	1.00	cp
k_{roe}	1.0	-	k_{rwe}	0.04	-
n_o	1.8	-	n_w	2.5	-
S_{wo}	0.57	-	S_{wi}	0 or 0.15	-
S_{wf}	0 or 0.28	-	B	6.5	-
P_{ct}	2.55	kpa			

For the saturation profile in Fig. 5.1, there is no sharp displacement front, such as that frequently observed in Buckley-Leverett flow. However, fronts have been observed in spontaneous imbibition experiments. Such fronts result because flow of the wetting phase cannot occur below a given saturation; flow does not occur until three-dimensional phase imbibition canals build up (Li, et al,1986). This has the effect of causing the front to have a finite saturation, and not proceed as a sloping front (Wardlaw and Li, 1988; Baldwin and Spinler, 1999). In order to account for the possibility of this occurrence, results were calculated using a saturation at the front with the value (S_{wf}) given in Table 5.1. The resulting curves are shown in Fig. 5.2. Again, the agreement between the two solutions is very good for all variables.

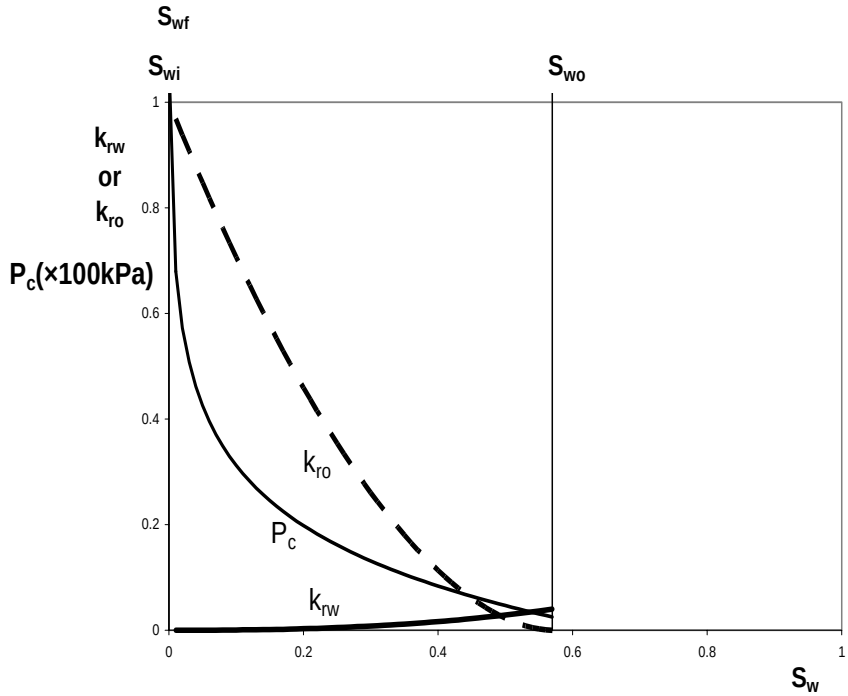

Fig.5.1a The relative permeability and capillary pressure curves used in the present study.

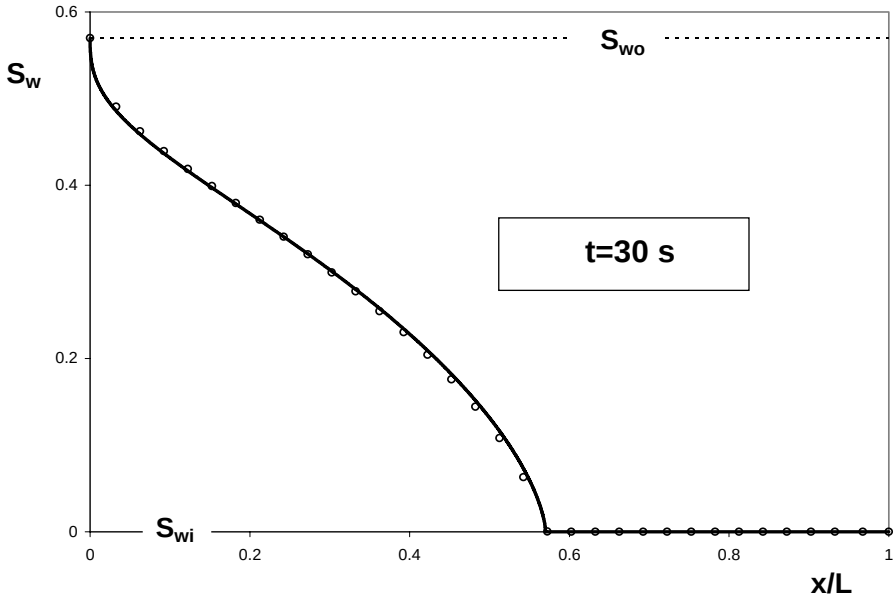

Fig.5.1b The saturation profile at a time of 30 seconds for the case where the initial water saturation is zero and the water saturation at the front is zero. The solid line is the analytical solution; the open circles are the simulation.

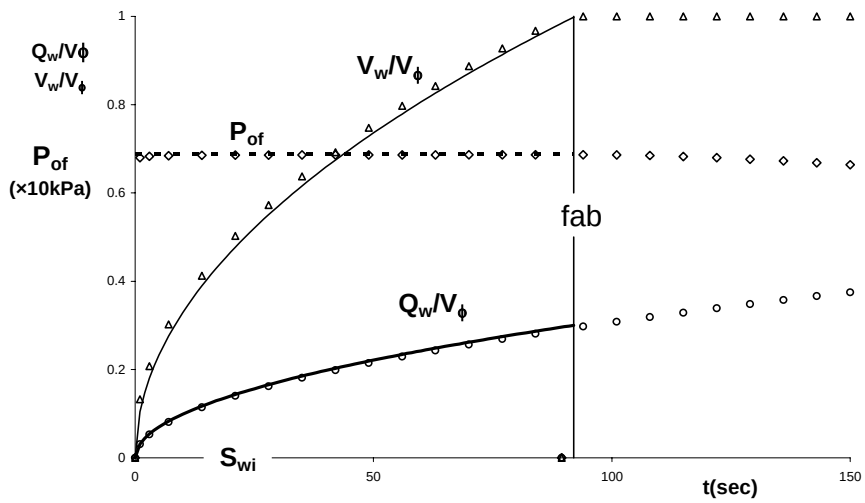

Fig.5.1c The production, invasion, and pressure histories for the case where the initial water saturation is zero and the water saturation at the front is zero. The solid lines are analytical solutions; the open circles are the simulations.

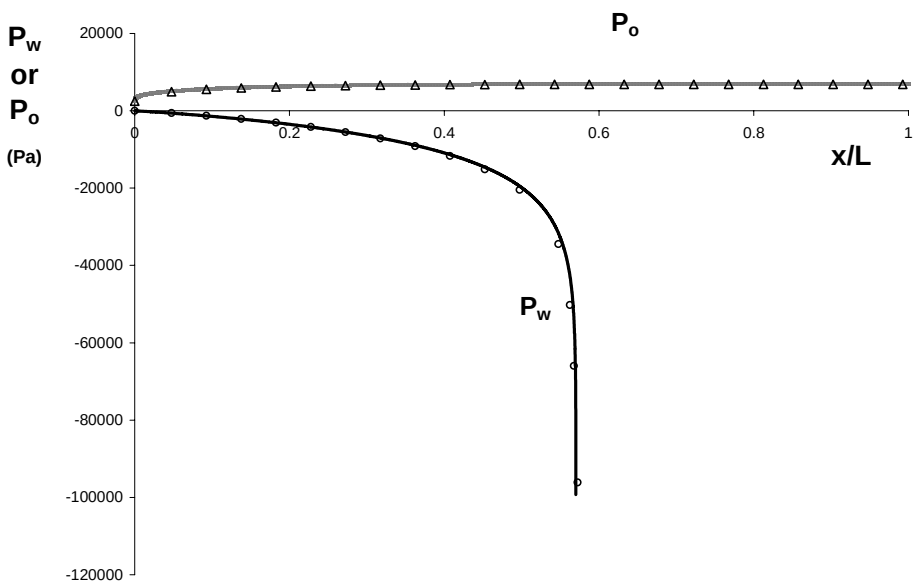

Fig.5.1d The pressure profiles at a time of 30 seconds for the case where the initial water saturation is zero and the water saturation at the front is zero. The solid lines are the analytical solutions; the open circles are the simulations.

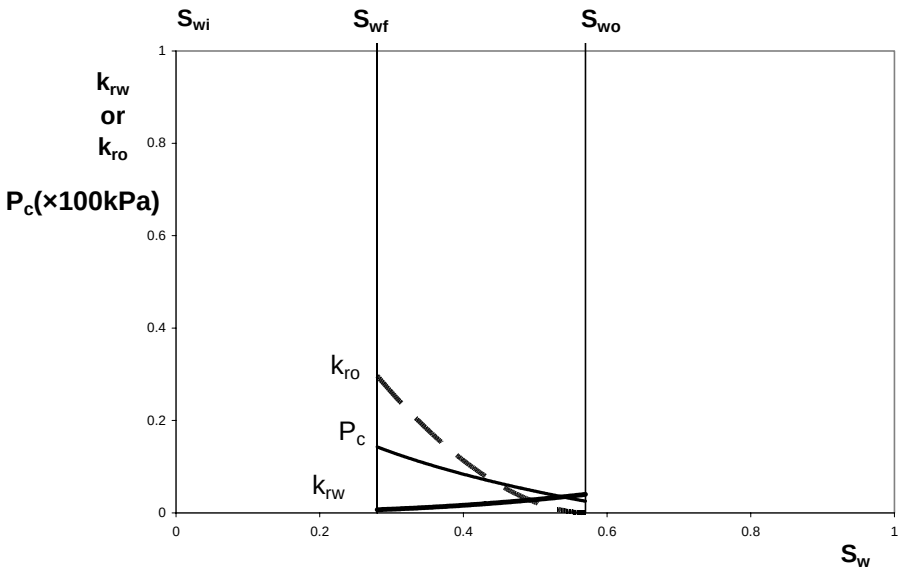

Fig.5.2a The relative permeability and capillary pressure curves truncated at $S_w = 0.28$. With S_{wi} (=0) less than S_w the saturation at the front is 0.28.

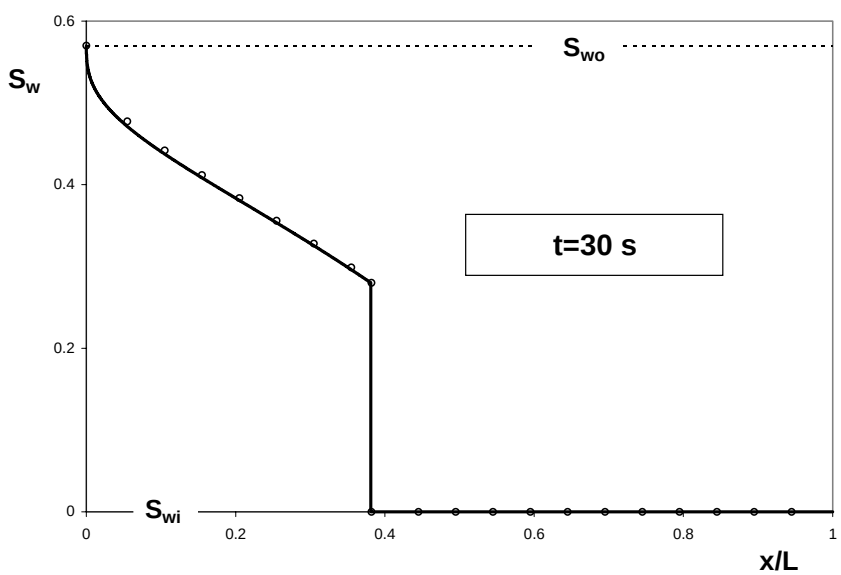

Fig.5.2b The saturation profile at a time of 30 seconds for the case where the initial water saturation is zero but the water saturation at the front is non-zero. The solid line is analytical solution; the open circles are the simulation.

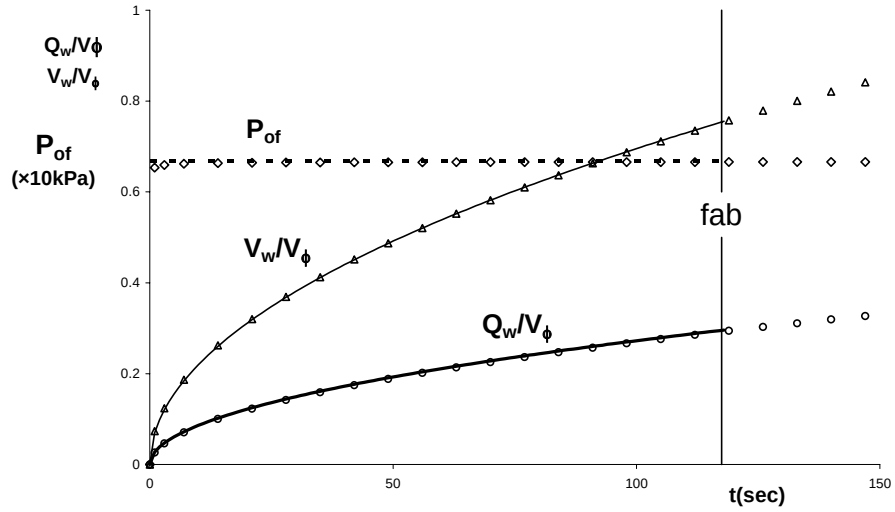

Fig.5.2c The production, invasion, and pressure histories for the case where the initial water saturation is zero but the water saturation at the front is non-zero. The solid lines are analytical solutions; the open circles are the simulations.

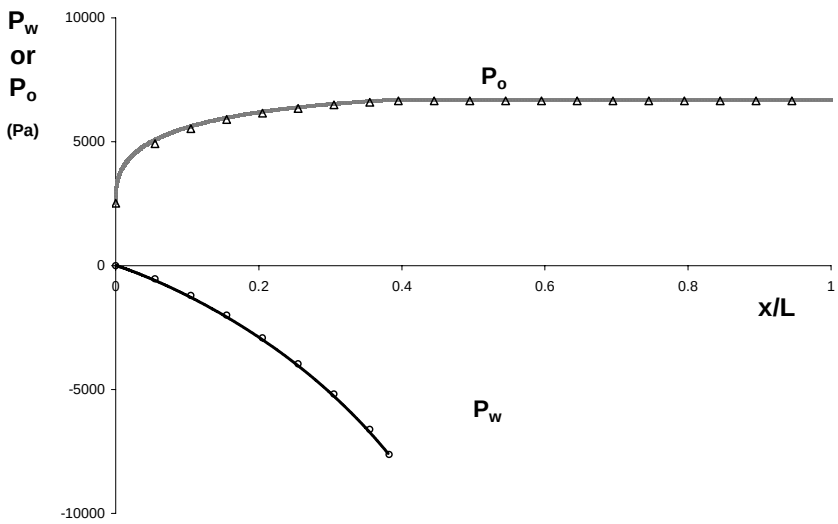

Fig.5.2d The pressure profiles at a time of 30 seconds for the case where the initial water saturation is zero but the water saturation at the front is non-zero. The solid lines are the analytical solutions; the open circles are the simulations.

The results in Fig.5.3 were obtained assuming that the front, wetting phase saturation, S_{wf}, was equal to the nonzero initial wetting phase saturation, S_{wi}. This is a common case when initial wetting phase is a continuous phase and is mobile if a pressure gradient is imposed. Because the

front in this case proceeds as a very shallow wedge, it appears that the wetting phase increases globally after the beginning of imbibition. The analytical solutions and simulation results agreed well except for the positions of the front. The disagreement (Fig.5.3c) is due to the difficulty for the simulation to precisely predict extremely small saturations.

For Fig. 5.4, the front saturation was assumed to be slightly larger than the irreducible value. This will occur if the initial saturation is less than or equal to the wetting phase saturation at which the mobility of the wetting phase is essentially zero, that is, at the beginning of imbibition, the wetting phase is not hydraulically continuous. For this case the excellent agreement of analytical solution and approximation is restored.

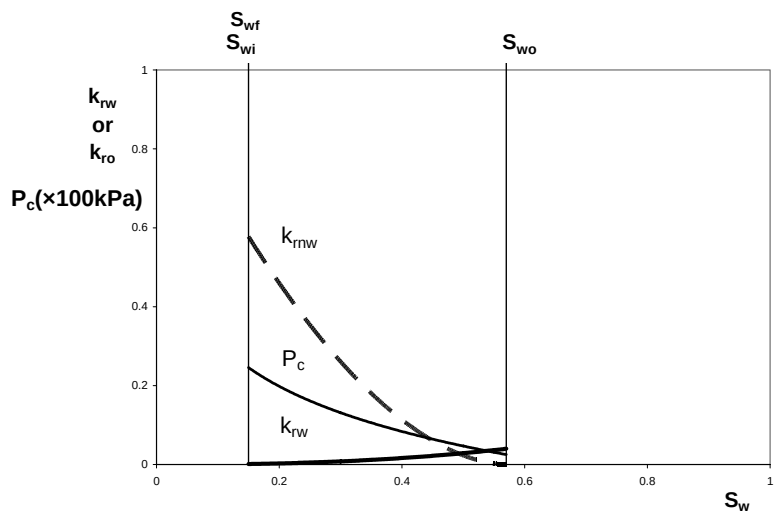

Fig.5.3a The relative permeability and capillary pressure curves for the case of non-zero initial water saturation. But is the relative permeability now truncated at 0.15 or equal to zero at .15?

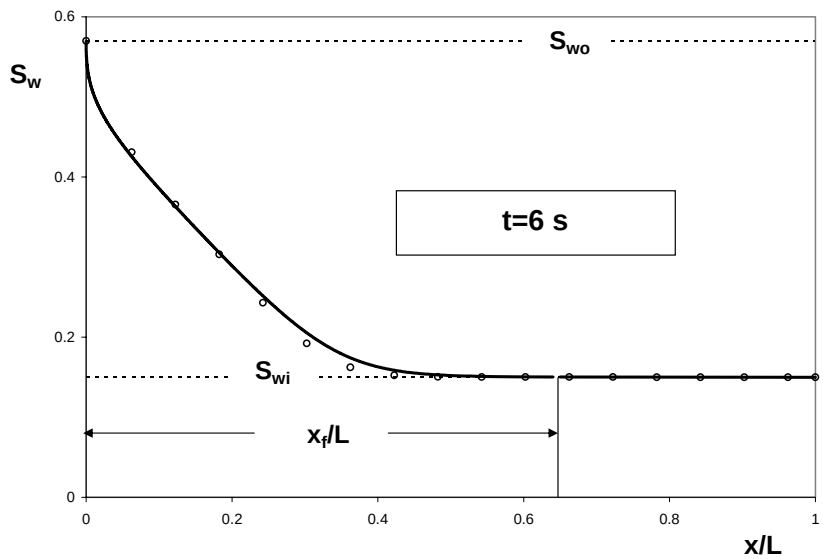

Fig.5.3b The saturation profile at a time of 6 seconds for the case where the initial water saturation is non-zero and the water saturation at the front is equal to this initial value. The solid line is the analytical solution; the open circles are the simulation.

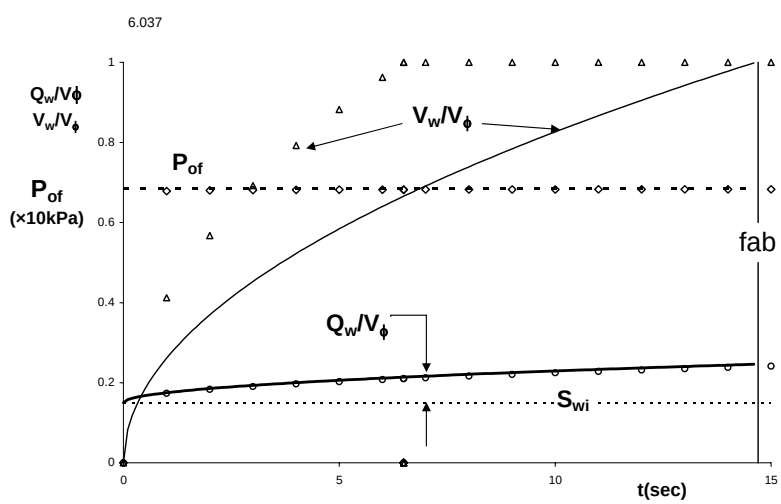

Fig.5.3c The production, invasion, and pressure histories for the case where the initial water saturation is non-zero and the water saturation at the front is equal to this initial value. The solid lines are the analytical solutions; the open circles are the simulations. The agreement is excellent except for the invasion history. The reason for this is that the simulation is very sensitive to truncation errors for the case where a cone-like front results in low saturations.

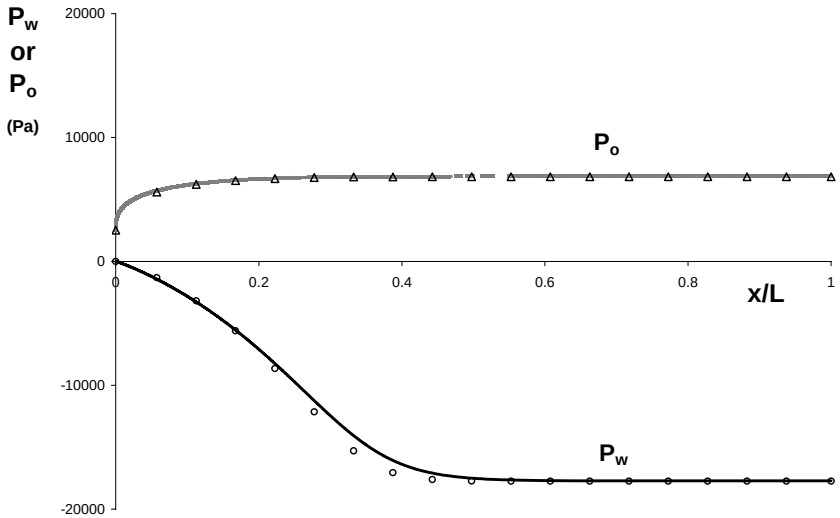

Fig.5.3d The pressure profiles at a time of 6 seconds for the case where the initial water saturation is non-zero and the water saturation at the front is equal to this initial value. The solid lines are the analytical solutions; the open circles are the simulations.

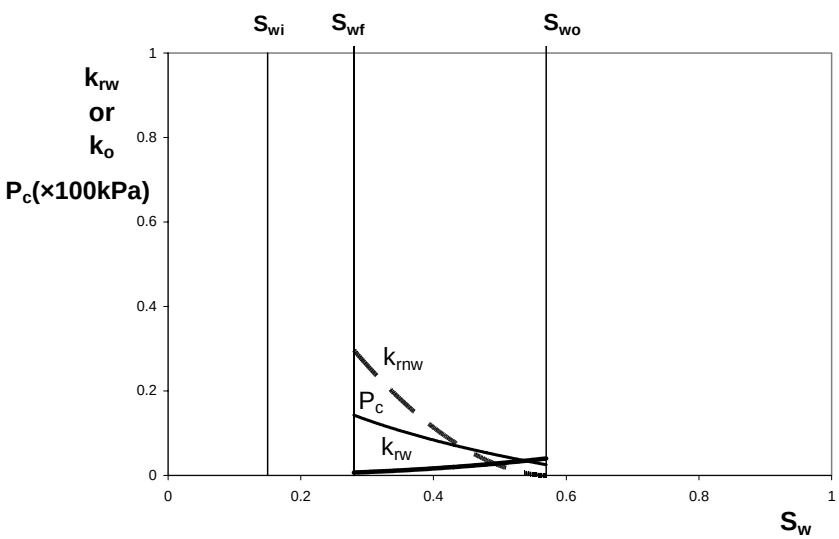

Fig.5.4a The relative permeability and capillary pressure curves for the case of non-zero initial water saturation and a saturation at the front greater than this initial water saturation. (and presumably the relative permeability was truncated at 0,28)

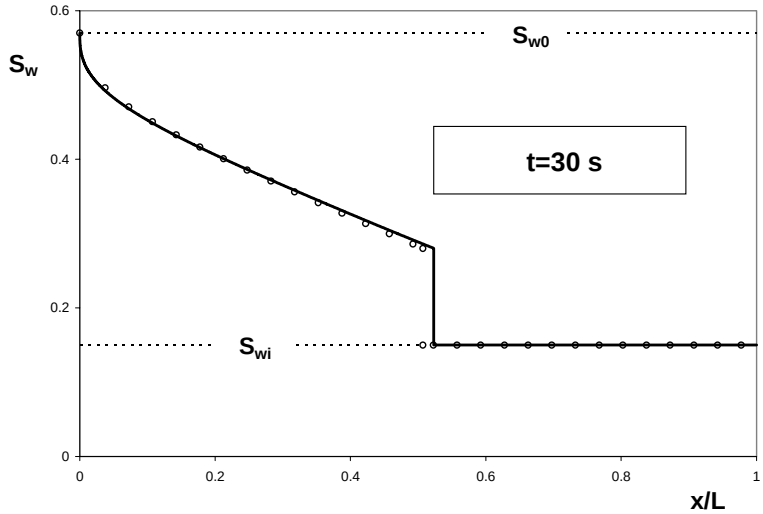

Fig.5.4b The saturation profile at a time of 30 seconds for the case where the initial water saturation is non-zero (17%?) and the water saturation at the front (28% and equal to the relative permeability cut-off) is greater than this initial value. The solid line is the analytical solution; the open circles are the simulation.

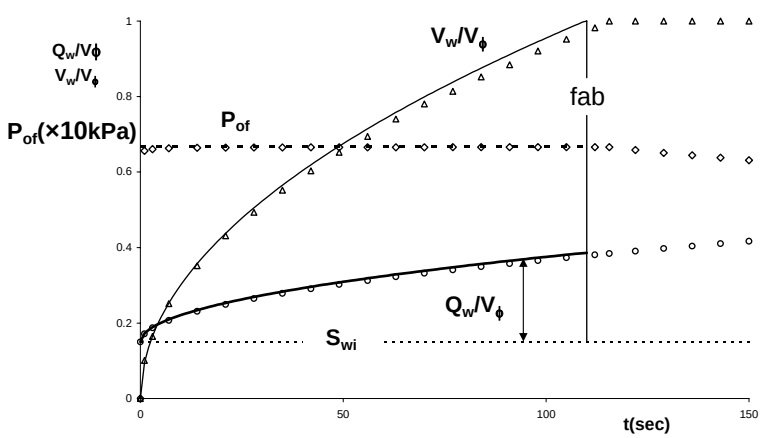

Fig.5.4c The production, invasion, and pressure histories for the case where the initial water saturation is non-zero and the water saturation at the front is greater than this initial value. The solid lines are the analytical solutions; the open circles are the simulations.

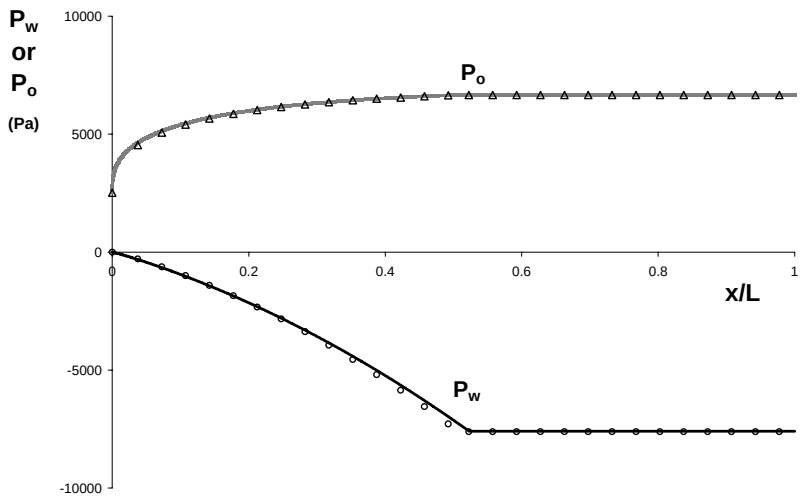

Fig.5.4d The pressure profiles at a time of 30 seconds for the case where the initial water saturation is non-zero and the water saturation at the front is greater than this initial value. The solid lines are the analytical solutions; the open circles are the simulations.

Results and Discussion

An analytical solution has been presented for one-dimensional, linear, counter-current, spontaneous imbibition into a porous sample for the period up to when the invading phase contacts the dead-end of the sample. The analytical method will work for arbitrary relative permeability, capillary pressure, and other sample parameters.

CONCLUSIONS

1. Advances have been made in interpretation and analysis of saturation and surface areas from 2-D images from thin sections.
2. A Hub and Spoke model of imbibition has been developed.
3. Experimental results for production of both gas and oil by spontaneous imbibition have been matched by simulation. Results can be used to predict saturation and pressure profiles by numerical simulation.
4. An extensive imbibition data set has been obtained and correlated for recovery of 43 cp oil for a wide range of wetting phase viscosities.
5. Analytic solutions for spontaneous imbibition have been verified by numerical simulation.

REFERENCES

Baldwin, B.A., and Spinler, E.A., In-situ Saturation Development during Spontaneous Imbibition, *Proceedings of the International Society of Core Analysts*, SCA-9922, 1999,1-11

Bradford S., and Leij F., Estimating area for multi-fluid soil systems, *Journal of Contaminant Hydrology*, 27 (1997) 83-105.

Gladkikh M., Jain V., Bryant S., Sharma M.M., Experimental and theoretical basis for a wettability-interfacial area-relative permeability relationship, SPE Annual Conference and Exhibition, Denver, CO, USA, 5-8th October, 2003.

Jain V., Bryant S., and Sharma M.M., "Influence of wettability and saturation on liquid-liquid interfacial areas", *Environ. Sci. Technol*. 2003, 37, 584-591.

Kim H., Rao S.C., and Annable M.D., "Determination of effective air-water interfacial area in partially saturated porous media using surfactant adsorption", *Water Resources Research*, 33, 2705-2711, Dec 1997.

Li,Y., Laidlaw, W.G., and Wardlaw, N.C., Sensitivity of drainage and imbibition to pore structures as revealed by computer simulation of displacement process, *Adv. Colloid Interface Sci.* 26, 1986, pp.1-68

Li, Y., Ruth, D.W. and Morrow, N.R., Similarity solution for linear counter-current spontaneous imbibition, *Journal of Petroleum Science and Engineering*, 39, 2003, pp.309-326.

Morrow, N.R., "Physics and thermodynamics of capillary action in porous media", *I&EC* 1970.

Morrow, N.R. and Mason, G., "Recovery of oil by spontaneous imbibition", *Current Opinion in Colloid and Interface Science,* 6, 2001, 321-337.

Scheafer C., DiCarlo D., Blunt M.J., Determination of water –oil interfacial area during 3-phase gravity drainage in porous media, *Journal of Colloid and Interface Science*, 221, 308-312 2000a

Scheafer C., DiCarlo D., Blunt M.J., Experimental measurement of air-water interfacial area during drainage and secondary imbibition in porous media , *Water Resources Research*, 36 , 885-890, Apr 2000b

Russ, John C. and Dehoff, Robert T., *"Practical Stereology"*, 2nd edition, Kluwer Academic/Plenum Publishers, New York, NY, 2000.

Ruth. D.W., Morrow, N.R., Li, Y., and Buckley, J.S., 2000, A simulation study of spontaneous imbibition, Proc. Int. Sym. of SCA, Abu Dhabi, U.A.E, Paper 2000-24.

Underwood, Ervine E., *"Quantitative Stereology"*, Addison-Wesley Publishing Company, Reading, MA, 1970.

Wardlaw, N.C., and Li, Y., Fluid Topology, Pore Size and Aspect Ratio during Imbibition, *Transport in Porous Media,* 3, 1988, 17-0.34

Washburn, E.W.: "The Dynamics of Capillary Flow," *Phys. Rev*. (1921) **17**, 273-283.

Zhang, X., Morrow, N.R., and MA, S., Experimental verification of a modified scaling group for spontaneous imbibition. *SPE Reservoir Engineering*, Nov. 1996, pp.280-285.